Estimating fat, paste and gas in a proving puff pastry by MRI - Method and simulation results

Guylaine Collewet, Vincent Perrouin, Cécile Deligny, Jérôme Idier, Tiphaine Lucas

Estimating fat, paste and gas in a proving puff pastry by MRI – Method and simulation results

Guylaine Collewet[1,2], Vincent Perrouin[1,2], Cécile Deligny[1,2], Jérôme Idier[3], Tiphaine Lucas[1,2]

1 : IRSTEA, UR TERE, 17 avenue de cucillé, CS 64427, 35044 Rennes, France
2 : Université Européenne de Bretagne, France
3 : IRCCyN CNRS, F-44300 Nantes, France

1 Introduction

The aim of the method presented in this paper is to characterize the development of the structures of puff pastries during proving. Puff pastries are made of layers of fat and dough, which is itself composed of paste and gas. During the proving, the dough is expanding, its gas fraction is increasing and gas bubbles are developing. It is interesting to observe the evolution of the expansion which can be characterized in different ways. First of all, it is important to detect the layers of fat since they play a significant role in the development of the pastry. For example, it is interesting to determine whether they are continuous or not. It is also interesting to measure the evolution of the gas fraction of the different layers of dough, delimitated by the layers of fat, to detect the potential formation of large bubbles and to observe if they develop in specific areas such as near or far from the layers of fat.

Magnetic Resonance Imaging (MRI) is an imaging technique which meets most of the requirements for this application. First of all it is a non-invasive technique which is mandatory to observe the development of the fragile and highly deformable structures. Moreover, by choosing an appropriate acquisition protocol along with its parameters, it is possible to obtain a good contrast between fat, paste and gas. The size of a pastry grows approximately from 60x100x5 mm^3 at the beginning of the proving to 60x100x25 mm^3 at the end of the proving. This fits also the MRI potentialities. However, in the case of this application, the use of MRI faces two problems which are the relative low value of the signal to noise ratio (SNR) and the relative small spatial resolution regarding the size of the structures we want to observe. This is due to several reasons. First of all, and particularly at the end of the proving, the dough contains much gas that gives no signal. The signal is thus decreasing in the dough during proving. Moreover, the SNR and the resolution are linked by the following relations:

$$SNR \propto \Delta V \sqrt{t_{acq}} \tag{1}$$

$$\Delta V = \frac{L_x L_y}{N_x N_y}\, e \tag{2}$$

$$t_{acq} = TR\, N_y N_{acc} \tag{3}$$

where ΔV is the elementary volume which corresponds to one voxel[1] of the image, L_x and L_y are the size of the field-of-view in both directions of the image-plane, e is the thickness of the virtual slice, N_x and N_y are the number of the voxels in the image (number of lines and columns). t_{acq} is the acquisition time, N_{acc} is the number of the repetitions of the acquisitions before averaging the signal, in order to reduce the noise and TR is the so-called repetition time which also influences the contrast in the images.
Thus, the values of SNR, ΔV and t_{acq} are linked and the choice of the acquisition parameters is a compromise between getting a high SNR, a high spatial resolution (ie a small ΔV) and a short t_{acq}. One way

[1] In MRI one picture element, or pixel, of the image is called a voxel since the signal is the sum of the signals of all the protons located in an elementary volume

to increase the SNR would be to increase the acquisition time. However, as we want to follow the expansion of the dough, the acquisition time should be limited in order to avoid movement artefacts in the images. Concerning the value of ΔV it would be interesting to set it such that the thin layers of fat would be represented by a line thick of a few pixels in the images. However, a too small value of ΔV would imply a low value for SNR. Finally, along with the intrinsic limitations of MRI, these constraints will set the values of ΔV on the order of 1mm^3. Since the thickness of the layers of fat are in the order of 0.1 mm, this leads to partial volume effects, that is, each voxel of the image will contain a mixture of fat and dough. The same phenomenon will be observed with dough and gas, since the size of the smallest bubbles does not exceed the resolution of the image. Thus, the MRI images for this application will present relatively low SNR combined with a strong partial volume effect. As this will be detailed in the paper, this led us to develop a method able to estimate in each voxel the quantity of each component, fat, paste and gas while adding some spatial regularization in order to reduce the effects of the noise.

This report is organized as follows: firstly we will present the model of the MRI signal. As each voxel corresponds to a mixture of components, the signal will be modelled as the sum of the signal of each component. This will lead to the estimation of several unknowns for each voxel which are the proportions of each component. This implies the use of several images acquired with different acquisition parameters and also the knowledge of "reference signals" for each component. The estimation of the unknowns comes down to find the solutions of a criterion composed of the squared difference between the data and the model. In order to get rid of the unwanted effects of the noise, this criterion is completed with a regularization term imposing solutions with a relative spatial smoothness. The optimization algorithm used to minimize this criterion is detailed. Then several simulation results are presented. First of all the choice of realistic numerical values corresponding to the targeted application is presented. Then the setting of the parameters of the algorithm is detailed. Finally, the results are divided in two parts. First of all we explored the performance of the method with the hypothesis that reference signals are perfectly known. Then we detail results including the uncertainty on these parameters using Monte-Carlo simulations.

2 Measurement method

2.1 Signal model

The model of the MRI signal depends on the acquisition protocol. Indeed, this imaging modality offers different ways to acquire a signal. In our case of interest, two kinds of protocol could be considered. The first one is the "spin echo" protocol (SE) which provides a signal with the same phase whatever the components. The amplitude depends on the characteristics of the component which allows distinguishing between fat and paste. The second one is the "gradient echo" protocol (GE) which is routinely used to quantify fat. Indeed, this protocol provides a signal the phase of which is different for fat. However, this protocol is prone to be sensitive to local magnetic field variations, which typically occur at the interfaces with gas. This leads to unexpected loss of the signal, especially in the dough where many small bubbles of gas are present. This would give images with no signal for the dough. For this reason we chose to use the SE protocol.

As explained in the introduction, we considered that each voxel contains a mixture of an unknown proportion of three components, fat, paste and gas. We made the hypothesis that the signal of each component did not vary with the localisation within the pastry, in other words that the signal of a voxel filled with fat or paste would not depend on the position in the pastry. When the sample is large regarding the size of the coil which acquires the signal, unwanted variations of the signal can be observed near the border. We assumed that, thanks to the small size of the sample and to its positioning in the centre of the coil, the signal could be considered as independent of the position. Thus, under these hypothesis, the signal s^*_{xkt}, for each voxel x, in absence of noise, at time t, with the set of acquisition parameters k can be modelized by:

$$s^*_{xkt} = \sum_{i=1}^{I} O_{ikt} p_{xit} \quad (4)$$

subject to

$$\sum_{i=1}^{I} p_{xit} = 1 \quad (5)$$

where I is the number of components, which will be set to 3 in the present study, $p_{xit} \in [0\ ,1]$ stands for the proportion of component i in voxel x at time t, $O_{ikt,}$ referred hereafter as "reference signals", corresponds to the signal of a voxel filled with component i at time t, with the set of parameters k. In the remainder of the paper i will be equal to f, p and g respectively for fat, paste and gas.

It is to be noted that the reference signals are subject to vary with time mainly because of the variation of the temperature. This implies for the targeted application that temperature should be measured along with the acquisition of the images. Since no metallic components should be used in the MRI system, optical fibres are used for that purpose.

In MRI, the signal of an image acquired with the parameters k corresponds to the modulus of a complex number, the real and imaginary component of which are added with a centered gaussian noise with the same variance σ_k^2. Thus the noise corruption of the MRI signal is not gaussian but follows a rician law. Taking this into account, under the non-reductive hypothesis of a phase equal to 0, leads to model the rician-noised signal s^R_{xkt}, where R stands for rician, as :

$$s^R_{xkt} = \sqrt{(s^*_{xkt} + n_{xkr})^2 + n^2_{xki}} \quad (6)$$

where n_{xkr} and n_{xki} are respectively the gaussian additive noise on the real and on the imaginary part of the complex signal for voxel x. For the sake of simplification, we will consider hereafter that the noise is not rician but gaussian and additive with a variance equal to σ_k^2. It can be shown that this hypothesis stands for $SNR > 3$ (Gudbjartsson & Patz, 1995). However, as it will been shown later, SNR can be lower than 3 in images of proving puff pastry which will lead to some bias of the results. The model s_{xkt} of the signal we used was the noise-free signal added with gaussian noise and expressed as :

$$s_{xkt} = s^*_{xkt} + n_{xk}, \quad (7)$$

where n_{xk} is a gaussian centered noise with variance σ_k^2.

The model of the signal being expressed, we are going to detail how we will estimate the unknowns.

2.2 Estimation of the unknowns

First of all, we considered that O_{ikt} can be measured separately and once for all using homogeneous block of fat and of paste. This point will be detailed later. Moreover, O_{ikt} will be set to 0 for gas, whatever the temperature, since this component gives no signal. Thus, the unknowns are p_{xit} which amounts, at one time t, to I images, i.e. $(I-1)X$ scalar unknowns given constraint (5) and noting X the number of voxels in the image. For the remainder of the paper, in order to lighten the notations, we will note the unknowns p_{xi}. This is possible since, as it will be explained later, the estimation will be realised separately for each time t. p_{xi} thus refer to the unknowns in the current image.

In order to build reliable estimates, we propose to acquire $K \geq I-1$ images using different values of parameters k. This is possible in MRI since different settings of the protocol parameters lead to different signal amplitude. This will lead to different values of O_{ikt}.

Moreover, in a view to reduce the noise, some regularization on the component proportions p_{xi} can also be introduced. However, it should be carefully designed, so that large variations of the signal be not penalized at the boundaries between distinct regions of the object namely the layers of fat and dough or large bubbles inside dough. In this paper, we adopt an approach so-called edge-preserving in the field of image restoration. More precisely we propose to estimate $\boldsymbol{p} = (p_{xi})$ using a penalized least-square approach:

$$\widehat{\boldsymbol{p}} = \arg\min_{\boldsymbol{p}} \mathcal{J}(\boldsymbol{p}) \tag{8}$$

where

$$\mathcal{J}(\boldsymbol{p}) = \sum_{k=1}^{K} \lambda_k \sum_{x=1}^{X} \left(s_{xkt} - \sum_{i=1}^{I} O_{ikt} p_{xi} \right)^2 + \gamma \sum_{c \in \mathcal{C}} \Phi(\|\boldsymbol{d}_c^t \boldsymbol{p}\|) \tag{9}$$

$\Phi(u) = \sqrt{\delta^2 + u^2}$ and $\|.\|$ denotes the usual L_2 norm. Parameters $\lambda_k$and γ are positive weights and δ is a scalar. $\mathcal{C}$ represents the set of pairs of adjacent pixels $c = \{y, z\}$ with $y < z$ for an arbitrary ordering. $\boldsymbol{d}_c$ is the $X \times 1$ finite difference vector such that $\boldsymbol{d}_c^t \boldsymbol{p} = \left[p_{y1} - p_{z1}, \ldots, p_{yI} - p_{zI}\right]^t$.The first term in (9) accounts for fidelity to data, the second term tends to decrease the noise in $\boldsymbol{p}$ while allowing rapid variations. Indeed, function Φ has a quadratic behavior near 0 and an asymptotically linear behaviour (see Figure 1). For large values of $\|\boldsymbol{d}_c^t \boldsymbol{p}\|$ that is for large values of differences between the vector proportion of adjacent pixels, the regularizing term will be lower than it would be using a quadratic regularization. This allows to penalize variations of $\boldsymbol{p}$ depending on the value of these variations.

Since Φ is strictly convex, it can be easily shown that $\mathcal{J}$ is strictly convex w.r.t. $\boldsymbol{p}$, and, therefore, a unimodal function of $\boldsymbol{p}$. However, The minimization of $\mathcal{J}$ is not trivial since $\mathcal{J}$ is not a quadratic function of $\boldsymbol{p}$. We used a non-linear conjugate gradient (CG) algorithm such as the one detailed in (Labat & Idier, 2008) to minimize $\mathcal{J}$ w.r.t $\boldsymbol{p}$, subject to constraint (2). CG algorithm is iterative. We initialized the solution with the one that minimizes the first term in (9) which corresponds to a least-squares minimization. This is easily computable since it is separable (the solution for each voxel is independent from the others) . Then we iterated the CG steps until the norm of the gradient of $\mathcal{J}$ w.r.t $\boldsymbol{p}$ becomes sufficiently small, *i.e.* $\|\nabla \mathcal{J}(\boldsymbol{p})\| \leq \varepsilon$.

One key point of our method is the choice of the hyperparameters λ_k, γ and δ. According to the probabilistic interpretation of criterion, $\lambda_k$corresponds to the inverse of the noise variance for the *k*th image. The noise variance can be estimated directly from the images using the method proposed in (Nowak, 1999). Two parameters remain to be adjusted. Their settings are made using simulations results as this will be developed later on. As these simulations require some realistic numerical values for all the variables, we first detail how we determined them.

2.3 Realistic numerical values and choice of the parameters k

In the case of SE protocol the reference signals can be written as:

$$O_{ikt} = G \rho_{it} e^{-TE_k/T_{2it}} \left(1 - e^{-TR_k/T_{1it}}\right), \tag{10}$$

where G represents the global gain of the acquisition system, ρ_{it}, T_{2it} and T_{1it} respectively the proton density, transversal and longitudinal relaxations times for component i at time t. TE_k is the so-called "echo time" and is a parameter chosen by the user, as well as the values of the repetition time TR_k. Preliminary measurements on a block of fat and a block of paste showed that there was not much difference between the

T_1 of paste and fat whatever the temperature which is the physical parameters that varies with time and that is susceptible to make the relaxation times vary. T_1 varied from 190 ms for paste and 175 ms for fat at 15°C, i.e. at the beginning of the proving, to 236 ms for paste and 230 ms for fat at 30°C, i.e. at the end of the proving. On the contrary the values of T_2 were different: T_2 was around 23 ms for paste whatever the temperature and varied from 37 ms at 15°C to 82 ms at 30°C for fat. This led naturally to the choice of T_2-weighted contrast images, that is images with different values of TE_k. It is to be noted that this can be done without increasing the acquisition time since the acquisition of at least 2 images can be achieved using so-called "multi spin echo sequences". Regarding the constraints of our MRI system, the only sequence available was a SE sequence with maximum two echoes.

In order to choose the best TE_k we computed the Cramer-Rao bound for the first term of equation (4), that is we ignored the regularisation term at this stage. Measurements on a block of fat and a block of paste were realized at different temperatures using a spin echo sequence with different TE. This led to the estimation of T_{2t} and $M_{0t} = G\rho_t\left(1 - e^{-TR/T_{1t}}\right)$ for the fat and for the paste. Thanks to these values we computed Cramer-Rao bounds for different combinations of TE_1 and TE_2. We chose to determine the best TE_k for the temperature at the end of the proving (30°C). The lower Cramer-Rao bound for the estimation of fat and paste was for $TE_1 = 7$ ms and $TE_2 = 32$ ms.

The other acquisition parameters were set as follows: we set the field of view to 40 x 160 mm^2 which is a bit larger than the maximum size of the pastry at the end of the proving. The resolution was set to 0.5 x 0.5 mm^2 with a slice thickness of 3 mm. This led to a number of lines $N_y = 40/0.5 = 80$. The other parameters were set so as to get acceptable SNR and acquisition time. The rate of dough expansion was evaluated by MRI in order to determine the maximum acquisition time. It appeared that at the beginning of the proving when the expansion is the fastest and presents a linear behaviour with time, the height of a puff pastry with 4 layers of fat increased by 10 mm per hour. We decided that the increase in height during an acquisition should be less than 1 mm and the maximum acquisition duration was set to 5 minutes. Regarding theses constraints TR_k was set to 400 ms for $k = 1$ and 2 so as to get a relatively high level of the signal regarding equation (10). The number of accumulations N_{acc} was 9 so as to lead to an acquisition time $t_{acq} =$ 4mn 48 sec.

Figure 2 shows the reference signals of fat for these two TE values in function of the temperature. We approximated the evolution with the temperature with a polynomial function of order 2. For the paste, a dedicated experiment not detailed here, led us to consider that the reference signals did not vary, neither with the temperature nor the time and we used the values of 325 and 60 for TE_1 and TE_2 respectively.

We also acquired images with these parameters in order to measure the level of the noise in these conditions. The variance of the noise was estimated using the method proposed in (Nowak, 1999). We measured a variance equal to 12.25.

We then used these values to characterize the performance of our method. The results are presented hereafter.

3 Results and discussion

First of all we set the values of the regularisation parameters γ and δ and then we ran simulations in order to measure the performances. This last aim was reached in two steps. First, we considered that the signal references were perfectly known and we investigated the errors due to the noise and to the algorithm. We focused mainly on the comparison of the mean errors since one of the outputs of the image analysis would be mean quantities, of gas in dough layers for example. In a second part, we investigated the uncertainties on the results due to the uncertainties on the reference signals. We focused on the variability of the mean errors but also of the contrast in the image in order to assess if the different structures could easily distinguished by visual inspection. Finally, we used the contrast information to determine the minimum size of fat layer that can be expected to be visualised.

3.1 Setting of the values of γ and δ

We ran successive simulations with γ varying from 500 to 10000 by steps of 500 and δ varying from 0.05 to 0.6 by steps of 0.05. The set of values for γ was chosen empirically since no probable value can be inferred *a priori*. On the contrary, the value for δ can be compared with the value of $\|\boldsymbol{d}_c^t \boldsymbol{p}\|$ which corresponds to the difference between the component proportion of one voxel and of the voxel of the corresponding neighbourhood $\mathcal{C}$. Indeed δ can be considered as a threshold above which the Φ function is no more quadratic. As p_{xi} represents component proportion $\in [0\ ,1]$, we chose values from 0.05 to 0.6.

The simulations were led on virtual Danish pastries, simplified to a basic structural element composed of a unique layer of fat surrounded by an homogeneous dough. The thickness of the fat layer was set to 200, 100 or 50 µm which corresponds to an ideal four, eight and sixteen layers pastry for an initial thickness of fat representing one third of the total thickness of the pastry. The reference signals of fat were computed considering either 22°C at the beginning of the proving or 30°C at the end. Likewise, the gas proportion in dough was set at either 20% or 80% in order to cover the range of variations during proving (see Figure 4, especially maps of gas proportions); in the latter case, some bubbles full of gas, of different sizes were also added: 3.5×3.5 mm^2, 3×3 mm^2, 2.5×2.5 mm^2, 2×2 mm^2 and 1.5×1.5 mm^2 (see Figure 5).

The choice of the best couple of γ and δ was made upon three criterions. First of all we computed for each simulation run the sum of the square errors of the fat, the paste and the gas, noted E:

$$E = \sum_{i=1}^{I} \sum_{x=1}^{X} \sqrt{\frac{(p_{xi} - \hat{p}_{xi})^2}{X}} \qquad (11)$$

where p_{xi} and $\hat{p}_{xi}$ are respectively the actual and the estimated proportion of component i in voxel x. As the algorithm is iterative, the computation time until the convergence of the algorithm was variable. The simulations were run on a Intel® Core™ i7 CPU M640@2.80GHz. We also took this time into consideration in order to optimise both the accuracy of the estimation and the computation time. However, as the hypothesis on the noise was not valid for the zones with low SNR, we could not rely only on the value of E to choose the values of γ and δ . That is why we also used the observation of the estimated images in order to definitively choose the best couple of value for γ and δ. In other words, the values of E and of the computation time were indicators of acceptable values and the observation did the final cut.

Figure 3 shows the evolution of E in function of the computation time, i.e. in function of the number of the iterations of the algorithm, for the case with four layers of fat at the beginning and the end of the proving. This evolution showed a decrease in function of the computation time with an asymptotic behaviour when the computation time increased. Regarding the value of E, increasing the computation time is not worth above about 15 sec in our case. We observed several images obtained with different couples of values around this computation time value and we chose $\gamma = 6500$ and $\delta = 0.35$. Figure 4 shows the result maps of proportions calculated using these values of parameters for a 4 layers pastry at the beginning of the proving. From top to bottom of the proportion of fat, paste and gas are represented and from left to right the ground truth, the initialisation of the solution, which corresponds to the solution without any spatial regularisation and the final estimation. Figure 5 corresponds to the same information for a pastry at the end of the proving.

First of all, it is clear from these figures that the regularized solutions were closer to the reality than the non-regularised solution. The values of E fell down from 0.45 to 0.18 for pastry at the beginning of the proving and from 0.32 to 0.22 at the end of the proving. Moreover the structural elements such as the layers of fat and the gas cavities at the end of the proving were better visualized. However, some undesired marbling effect appeared especially in the cartography of paste proportion. It was not possible to get rid of this effect

with any couple of values for γ and δ. This suggested that any such effect that would occur in the cartography of the proportion of paste calculated from real images should not be interpreted as a reality. This marbling effect did not affect the shape and dimensions of the fat layer which can be well visualized from the cartography of the fat proportion; it slightly modified the outlines of the large bubbles which can be however detected even when their size was as low as 2×2mm^2.

3.2 Performance of the method for various proportions of fat, paste and gas with a perfect knowledge of reference signals

In order to assess the performances of the method, we ran simulations firstly on objects with uniform proportions and secondly on a proving dough without fat with a variable gas fraction and an increasing number of voxels.

3.2.1 Case of objects with uniform proportions

Virtual objects considered in this part of the study (100×100 voxels) were homogeneous but presented different proportions of fat, paste and gas in their constitutive voxels. A configuration without fat was considered, both at the beginning and the end of proving, with respectively 20% and 80% of gas. These values were found as typical in the literature. The specific configuration of the fat layers, which only partially filled the voxel, was also considered, both at the beginning and the end of the proving. In this case, partial volume of fat-dough was set at 50-50%, which is representative of an ideal four layers pastry. We considered the temperature equal to 22°C and 30°C respectively at the beginning and the end of the proving. This led to four cases, the characteristics of which are summarized in Table 1. We ran simulations both with regularisation ($\gamma = 6500$ and $\delta = 0.35$) and without (γ =0). In order to be in the same conditions as for the pastries, we limited the number of iterations of the CG algorithm to 18 which corresponds approximately to the number of iterations used for the settings of γ and δ.

Table1.

	Moment of proving	Temperature (°C)	Fat	Paste	Gas
Partial volume of fat-dough	Beginning	22	50%	40%	10%
Dough	Beginning	22	0%	80%	20%
Partial volume of fat-dough	End	30	50%	10%	40%
Dough	End	30	0%	20%	80%

The proportions of each component were computed from these virtual objects. The mean errors B_i (i.e. the bias that is the difference between the actual and the estimated values) and the standard deviations of the errors A_i were computed for each component i and expressed in % with the following formulae:

$$B_i = 100\frac{1}{X}\sum_{x=1}^{X}(p_{xi} - \hat{p}_{xi}) \tag{12}$$

$$A_i = 100\sqrt{\frac{1}{X-1}\sum_{x=1}^{X}(p_{xi} - \hat{p}_{xi} - B_i)^2} \tag{13}$$

Figure 6 shows B_f, B_p, B_g, A_f, A_p and A_g with and without regularisation for the four cases defined in Table 1. In all the cases, the values of fat and gas were overestimated ($B_i < 0$), while the values of paste were underestimated ($B_i > 0$). The largest absolute values of B_i were found for dough alone and they were even larger at the end of proving where $B_f = -3\%$, $B_p = 6\%$ and $B_g = -3\%$. This was attributed to the low value of signal because of the high proportion of gas. Additionally, the model of the signal is less valid in this case since we made the hypothesis that the noise is Gaussian and additive, which can be considered as true only for high values of SNR.

For the layers of fat, i.e. partial volume of fat and dough, the results were slightly better at the end of proving. Indeed at the temperature of 30°C the signal of fat is higher, thus the SNR is higher too. Moreover, as the reference signal of paste does not vary with temperature, the contrast between fat and paste is higher at 30°C which leads to estimations less dependent on the noise. This also explains the difference in the values of A_i between the beginning and the end of proving. The estimations were more sensitive to the noise in the signal in the first case, because of the values of the reference signals. It is to be noted that the values of B_i were very similar with or without regularisation which means that the regularisation scheme did not add any bias to the results.

On the contrary A_f, A_p and A_g were far lower with regularisation than without no matter the case. This was expected since the regularisation scheme was designed to remove the unwanted effects of the noise. Levels of uncertainty as low as 1% were hence reached with regularization.

The results showed that the behaviour of the method was different depending on the stage of proving and on the proportions of the component. At the beginning of proving the reference signals of fat are lower which decreases both the SNR and the contrast between fat and paste. However the gas fraction is also low which compensates this disadvantage. At the end of proving, the reference signals of fat are higher but the proportion of gas is higher which tends to raise up the bias for the estimation of the proportion of paste. The results showed that regularisation improved the results but did not allow removing the bias.

3.2.2 Particular case of the proving of a dough without fat

It is particularly interesting to measure the amount of gas in the dough for example to assess the mean gas fraction in a particular area. This can be done by summing the proportion of gas in this area and dividing the result by the size of the area. The error depends both on the gas fraction and on the size of the area. In order to evaluate the errors in function of both variables we have simulated the proving of a dough with no fat. The initial surface was 4147 voxels, the final one was 15762. Thus, contrary to the results presented in the previous section the size of the area varied proportionally to the increase in the amount of gas in dough. The results presented here are without regularisation since it has been shown previously that regularisation does not bring any improvement on the mean error.

We chose to represent the evolution of the sum of fat, paste and gas in function of time (Figure 7). Indeed the sum of the proportion of fat and paste should be constant over time. For the paste the sum over time was decreasing with a loss of up to 30% at the end. On the contrary, the sum of the estimated proportion of fat which should be zero, was increasing. Finally the amount of gas was overestimated. The linear regression between estimated and actual gas proportion with an intercept forced to zero presented a determination coefficient of 0.98 and a slope of 1.05. This meant that the amount of air was overestimated by 5% in mean.

3.3 Sensitivity of the method regarding the uncertainty on the reference signals

As the method relies on the knowledge of the "reference signal" O_{ikt} we have studied the sensitivity of the method regarding the uncertainty on these constants. Several questions were addressed:

- What is the uncertainty on the estimation of the proportions of each component?

- How is the contrast between the layers of fat and the layers of dough affected by the uncertainty?
- What is the effect of the regularisation on these uncertainties?

For this application, as explained before and illustrated in Figure 2, it was considered that fat signal was varying with temperature regarding the following law:

$$O_{fjt} = a_j {\theta_t}^2 + b_j \theta_t + c_j \qquad (14)$$

and that the reference signal of paste was constant and was respectively equal to 325 and 60 a.u. for $j = 1$ and 2 respectively.
As the temperature was involved in the value of the reference signal of fat we considered an uncertainty in its measurement. It was considered as a law $\mathcal{N}(0, \sigma_\theta)$, noting $\mathcal{N}(\mu, \sigma)$ the gaussian law the mean of which is μ and the standard deviation is σ. This took into account both the uncertainty of the measurement of the temperature $\mathcal{N}(0{,}1°C)$, which is realised jointly with the acquisition of the images, and the variation of the temperature in the pastry estimated to $\mathcal{N}(0{,}1°C)$. This led to $\sigma_\theta = 1.4\ °C$. We neglected the variation of the temperature during the acquisition of the image. We also took into account the uncertainty on the coefficients a_j, b_j, c_j adjusted on a given experimental set (here 5 points) of signals acquired in the same condition as during proving. This led to a "model uncertainty" on O_{fjt} following a law $\mathcal{N}(0, \sigma_{fmj})$ with σ_{fmj} =1.6/100 O_{fjt} at the beginning of the proving and σ_{fmj} =2.7/100 O_{fjt} at the end of the proving. Moreover, we considered that the reference signal of fat has a spatial natural variation around the estimated mean value with a law $\mathcal{N}(0, \sigma_{fxj})$ with $\sigma_{fxj} = 3/100\ O_{fjt}$. Concerning the reference signals of the paste we considered thanks to a dedicated experiment not detailed here, that they did not depend on the process of proving and that their uncertainty followed a uniform law $\mathcal{U}(0, A_{pj})$ centered around 0 and with a width equal to A_{pj}. We took $A_{pj} = 8/100\ O_{pjt}$ whatever j and t. We also considered that the reference signal of paste has a spatial natural variation around the estimated mean value with a law $\mathcal{N}(0, \sigma_{pxj})$ with $\sigma_{pxj} = 6/100\ O_{fjt}$. Finally we took into account the uncertainty of the signal due to the noise.

We ran 1000 Monte-Carlo simulations following this scheme:

For one operating temperature θ_t :
Choose randomly one temperature θ_t in $\mathcal{N}(\theta_t, \sigma_\theta)$.
Choose randomly O_{fjt} in $\mathcal{N}(a_j {\theta_t}^2 + b_j \theta_t + c_j, \sigma_{fmj})$ for $j = 1$ and $j = 2$
Choose randomly O_{pjt} in $\mathcal{U}(O_{pj}, A_{pj})$ for $j = 1$ and $j = 2$
For each voxel in the image:
Choose randomly O_{fjtx} in $\mathcal{N}(O_{fjt,}\sigma_{fxj})$ for $j = 1$ and $j = 2$
Choose randomly O_{pjtx} in $\mathcal{N}(O_{pjt,}\sigma_{pxj})$ for $j = 1$ and $j = 2$
Simulate the signal using equation (6) with the above reference signals replacing O_{ikt} with O_{iktx} for $i = f$ and $i = p$ and using 12.25 for the standard deviation of the noise

The same virtual objects as those described in section 3.1 were used for this part of the study. We computed the mean errors B_i. We also computed the contrast to noise ratio, CNR, between the voxels containing fat, paste and gas, that is the voxels corresponding to the layers of fat, and the voxels containing only paste and gas, that is the dough. CNR was computed on the map of the proportions of fat. For the pastry at the end of the proving we computed also CNR between dough and large bubbles of gas. This was computed on the map of gas proportions.

We used the definition of the CNR proposed in (Song et al., 2004) . CNR_i between voxels belonging to two different domains noted $\mathcal{S}_1$ and $\mathcal{S}_2$ and measured on the image of the proportions i was defined as:

$$CNR_i = \sqrt{2}\frac{\mu_{x\in\mathcal{S}_1}(p_{xi}) - \mu_{x\in\mathcal{S}_2}(p_{xi})}{\sqrt{\sigma^2{}_{x\in\mathcal{S}_1}(p_{xi}) + \sigma^2{}_{x\in\mathcal{S}_2}(p_{xi})}} \quad (15)$$

It is difficult to define a universal threshold value for CNR below which the contrast is not be high enough relative to noise to distinguish between the two given structures. Moreover, the clearness of the images also depends on the size of the structures under study and the detectability of structures by the human eye also involves a priori knowledge such as expected shapes and localisation. For the contrasts between fat layers and dough, values between -0.7 and 6.4 were found. Figure 8 shows four examples of low contrasts between fat and dough, from 0.4 to 1.2. The dynamic of the display was between -0.5 and +0.5 (-0.5 is black, +0.5 is white). Thanks to these images we can consider that above a contrast equal to 1.2 it is possible to distinguish between the fat layer and the dough. Concerning the contrasts between gas and dough, higher values were found, between 2.5 and 5. Figure 9 shows examples of different gas maps with contrasts between gas and dough equal to 2.5, 3, 4 and 5. The dynamic of the display was between 0.7 and +1.2 (0.7 is black, +1.2 is white). We can see that the smallest bubbles can hardly be detected at contrast 3, easier above.

Results from the Monte-Carlo simulations were very different for the beginning and the end of proving.

For the end of the proving, Figure 10 shows the distribution computed over the 1000 simulated maps of fat proportion of the values of CNR_f between layers of fat and dough with and without regularisation. Figure 11 shows the same distribution for the values of CNR_g between dough and bubbles of gas computed on the maps of gas proportion. It is clear that regularisation increased the contrast between the different structures by a factor of 2 at least and that the uncertainty on the reference signals did not significantly modify the values of this contrast. With regularisation the contrasts were respectively around 6 and 4 for fat layers and bubbles of gas in dough. This can be considered as high enough to ensure the visual analysis of the structures.

These simulations also allowed us to evaluate the dispersion of the values of B_i due to the uncertainty of the reference signals. B_f, B_p and B_g, in the dough were respectively equal to -3.4±0.15, 6.7±0.7 and -3.3±0.6 both with and without regularisation since the bias is not dependent on this factor as seen before. This means that the uncertainty on the reference signals did not make the values of B_i vary very much at the end of proving.

Concerning the beginning of proving, the results showed a very high variability. Figure 12 shows the same distribution as Figure 10 for the beginning of proving. The contrasts were lower than at the end of the proving and reached in some cases small values, below the threshold value of 1.2. However it is to be noted that these cases are not very frequent in the case with regularization. These low values of contrast are due to the fact that the difference between the reference signals of fat and paste was lower than at the end of the proving. B_f, B_p and B_g, in the dough were respectively equal to –2.6±2.2, 3.9±4.9 and –1.2±2.8 both with and without regularisation. Although the mean of the bias were smaller than at the end of the proving, its dispersion was very high. This means that at the beginning of the proving the measurement of mean proportions should be considered with a higher uncertainty than at the end of the proving. This is due to the fact that the reference signals of fat vary much more with the temperature than at the end of the proving as can be seen in Figure 2. We can observe a higher dispersion of the contrast in the regularised case. In fact the mean of the dough, $\mu_{x\in\mathcal{S}_2}(p_{xi})$ in equation (15), and the variances in the fat layer and in the dough, $\sigma^2{}_{x\in\mathcal{S}_1}(p_{xi})$ and $\sigma^2{}_{x\in\mathcal{S}_2}(p_{xi})$, were quasi-constant over the simulation runs. On the contrary the mean in the fat layer, $\mu_{x\in\mathcal{S}_1}(p_{xi})$, varied in function of the reference signals, especially those of the fat. It varied from 0 to 0.5 without regularisation and from 0 to 0.3 with regularisation. As the values of the variances were smaller with regularisation, this made the contrast more sensitive to $\mu_{x\in\mathcal{S}_1}(p_{xi})$ and thus the dispersion of the values higher for the contrast.

The combined effects of the uncertainty on the reference signals and of the noise did not have the same consequence at the beginning and the end of the proving. The uncertainties were higher at the beginning. However in both cases the regularization significantly improved the contrast in the estimated images of proportions allowing in most cases the visualization of the structures.

3.4 Detectability of the fat layers

As stated in the previous section we determined a threshold on the contrast under which fat layers could not be distinguished. This led us to use this criterion to determine the thinnest fat layer that can be visualised. We considered here that the reference signals were perfectly known. Similar virtual objects as those described in section 3.1 were used for this part of the study. We simulated fat layers of from 10 to 130 µm by step of 10µm both at the beginning and at the end of the proving.

Figure 13 presents the variation of CNR_f in function of fat thickness together with a selection of maps of fat proportions. In these maps, black is used for the minimum value, white for the maximum value, and grey levels varying linearly/proportionally to the fat proportions in between. A fat layer was easier to distinguish when CNR_f increased. There was a slight difference in detectability, i.e; when CNR_f > 1.25, between the beginning and the end of proving, because the contrast between paste and fat increased during proving [27]. We considered that the layers between 40 and 50 µm thick could be detected with the naked eye at the beginning of proving, and between 30 and 40 µm at the end. The single value of 40 µm was retained in the subsequent analysis.

4 Conclusion

We developed a method to estimate the proportion of the components included in each voxel of a MRI image and this was applied to the characterization of Danish pastries during proving. The method was based on the modelling of the signal as a sum of the signal of each component weighted by their proportion. The estimated proportions were those which minimized a function that was the sum of the squared difference between the data and the model and a regularization that ensured the smoothness of the solutions. It required the a priori knowledge of two reference signals (fat and paste). The noise in MRI is Rician, however the method was based on the hypothesis of a Gaussian noise.

The choice of the parameters of the algorithm that set the weight of the regularization term in the criterion was determined using simulated images. Using these parameters, and assuming excellent estimations of the reference signals, we showed that, in the case of our application, the mean error (systematic bias) was similar with or without regularization and depended on the components and their proportion while the dispersion of the results was lower with regularization. Fat and gas proportions were overestimated while paste proportion was underestimated. The absolute values of the bias varied from less that 1% up to 6% depending on the component and on the time of proving. The errors were larger for high gas proportion, *i.e.* at the end of the proving because of the lower SNR. The standard deviation varied from 0.3% up to 1.5 %. These values are not very high and acceptable for the targeted application.

Monte-Carlo simulations showed that these results were not influenced very much by the uncertainty on the reference signals at the end of the proving. However larger uncertainties were found at the beginning of proving due to the values of the reference signals of fat. Indeed, at this stage of proving they were lower, decreasing the contrast between fat and paste, and they were also more sensitive to the value of the temperature. We computed the contrast-to-noise ratio and found that it was higher with regularization no matter the proving time. We showed that the regularization of the solutions did improve the visualization of the structures confirming the interest of this approach.

Finally we found that layer down to 40 µm thick could be easily distinguishable in fat maps.

As a perspective to this work, we will first test our method on actual MRI images of Danish pastries during proving. In order to improve our method and particularly to remove the biases, it would be interesting to take into account the fact that the noise is Rician and not Gaussian. This will lead to a different expression of the criterion to be minimized. Moreover we also intend to add constraints on the proportions which are in between 0 and 1.

5 References

Gudbjartsson, H., & Patz, S. (1995). The Rician Distribution of Noisy MRI Data. *Magnetic Resonance in Medicine, 34* (6), 910-914.

Labat, C., & Idier, J. (2008). Convergence of conjugate gradient methods with a closed-form stepsize formula. *Journal of Optimization Theory and Applications, 136* (1), 43-60.

Nowak, R. D. (1999). Wavelet-based Rician noise removal for magnetic resonance imaging. *IEEE Transactions On Image Processing, 8* (10), 1408-1419.

Song, X. M., Pogue, B. W., Jiang, S. D., Doyley, M. M., Dehghani, H., Tosteson, T. D., & Paulsen, K. D. (2004). Automated region detection based on the contrast-to-noise ratio in near-infrared tomography. *Applied Optics, 43* (5), 1053-1062.

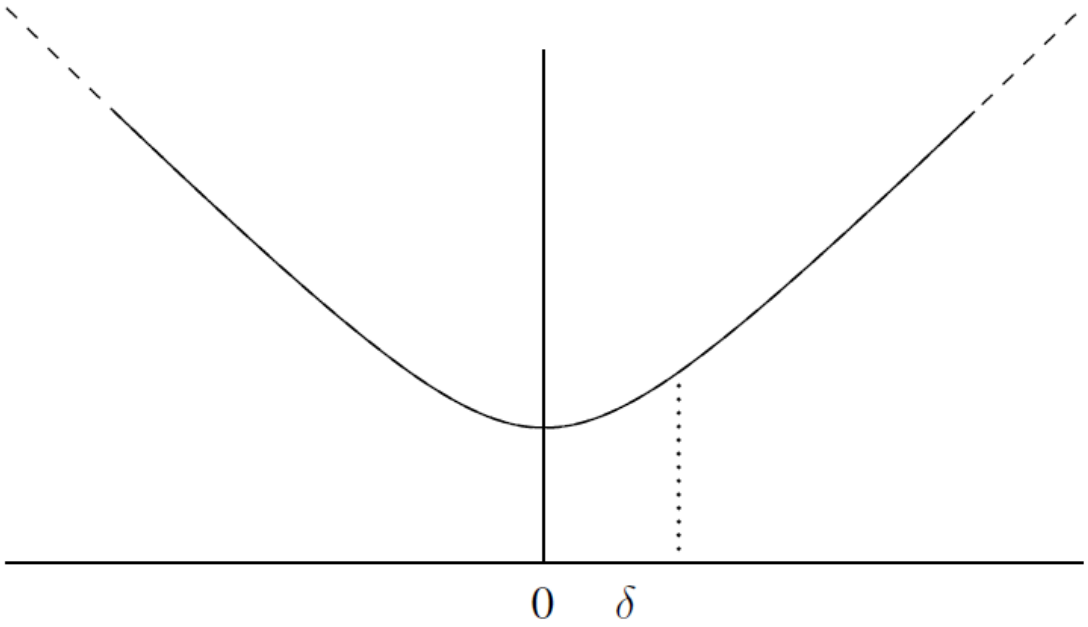

Figure 1: Variations of $\boldsymbol{\Phi(u) = \sqrt{\delta^2 + u^2}, \delta > 0}$

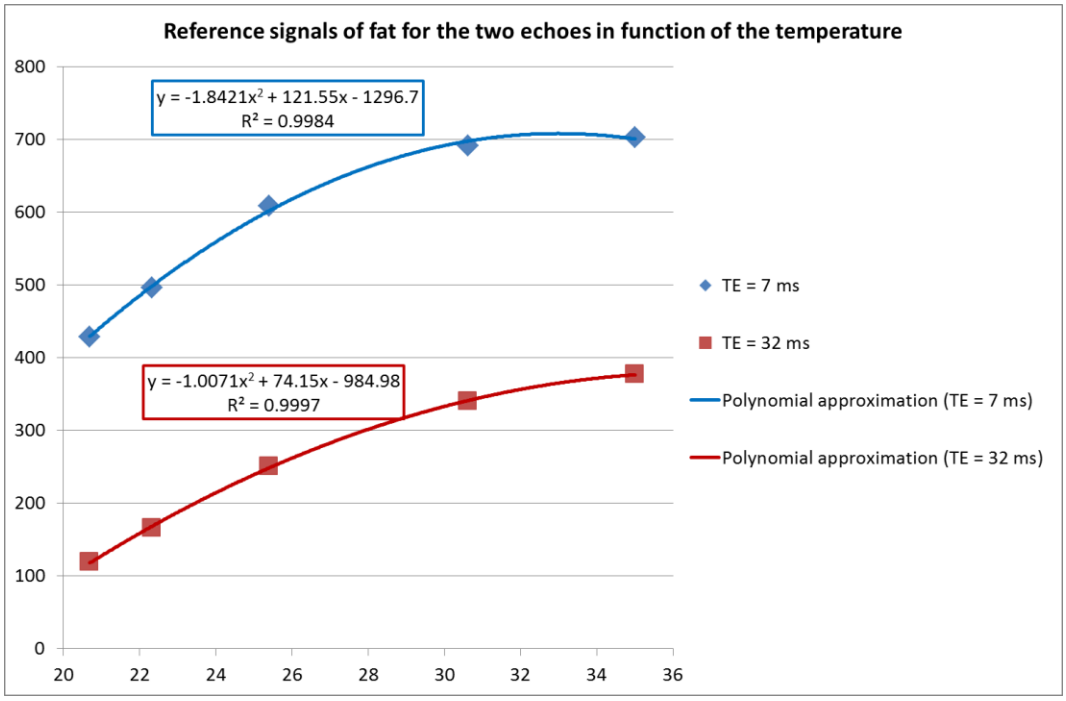

Figure 2: Reference signals of fat for the two echoes in function of the temperature and the corresponding polynomial approximations.

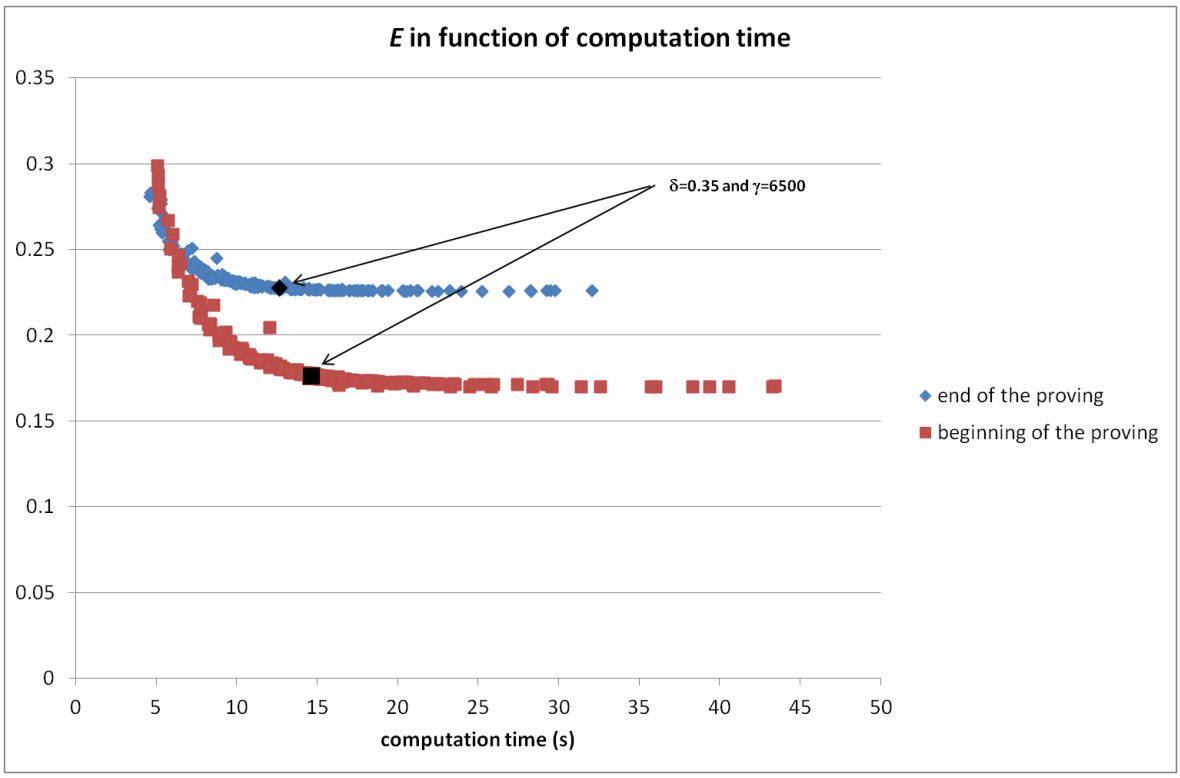

Figure 3: evolution of E for different combination of values for γ and δ in function of the computation time and for the beginning and the end of the proving. In black, the points corresponding to the values finally chosen. Case of a "four fat-layers" pastry

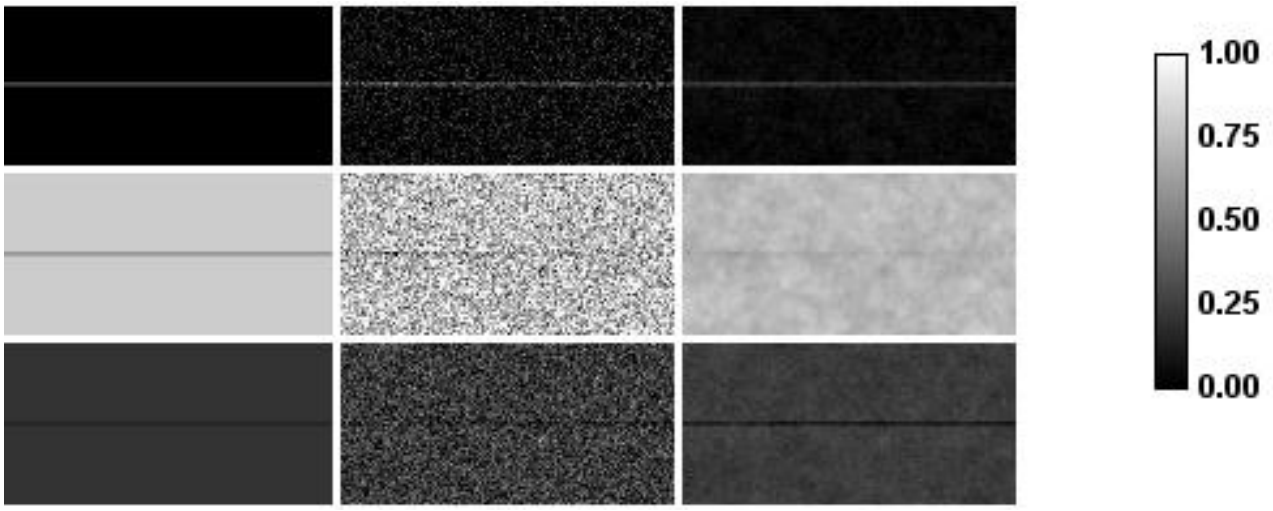

Figure 4: from top to bottom, proportion of fat, paste and gas. In the case of a pastry with a layer of fat whose thickness corresponds to a four-layers pastry and at the beginning of the proving. From left to right, the "ground truth" of the simulation run, the initialisation of the solution and the final estimation for $\gamma = 6500$ and $\delta = 0.35$.

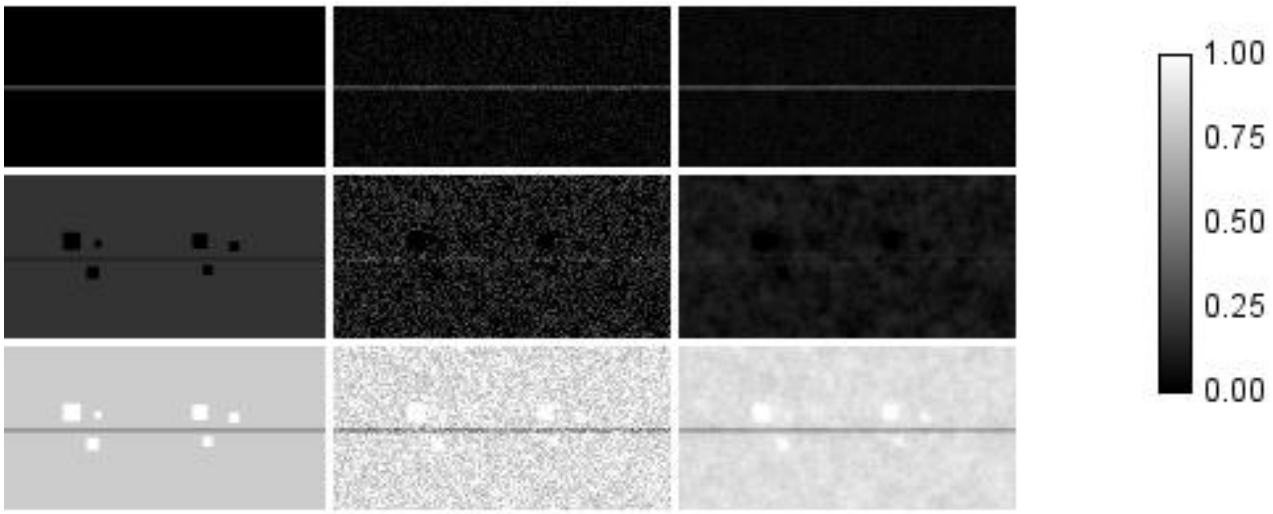

Figure 5: from top to bottom, proportion of fat, paste and gas. In the case of a pastry with a layer of fat whose thickness corresponds to a four-layers pastry and at the end of the proving. From left to right, the "ground truth" of the simulation run, the initialisation of the solution and the final estimation for $\gamma = 6500$ and $\delta = 0.35$.

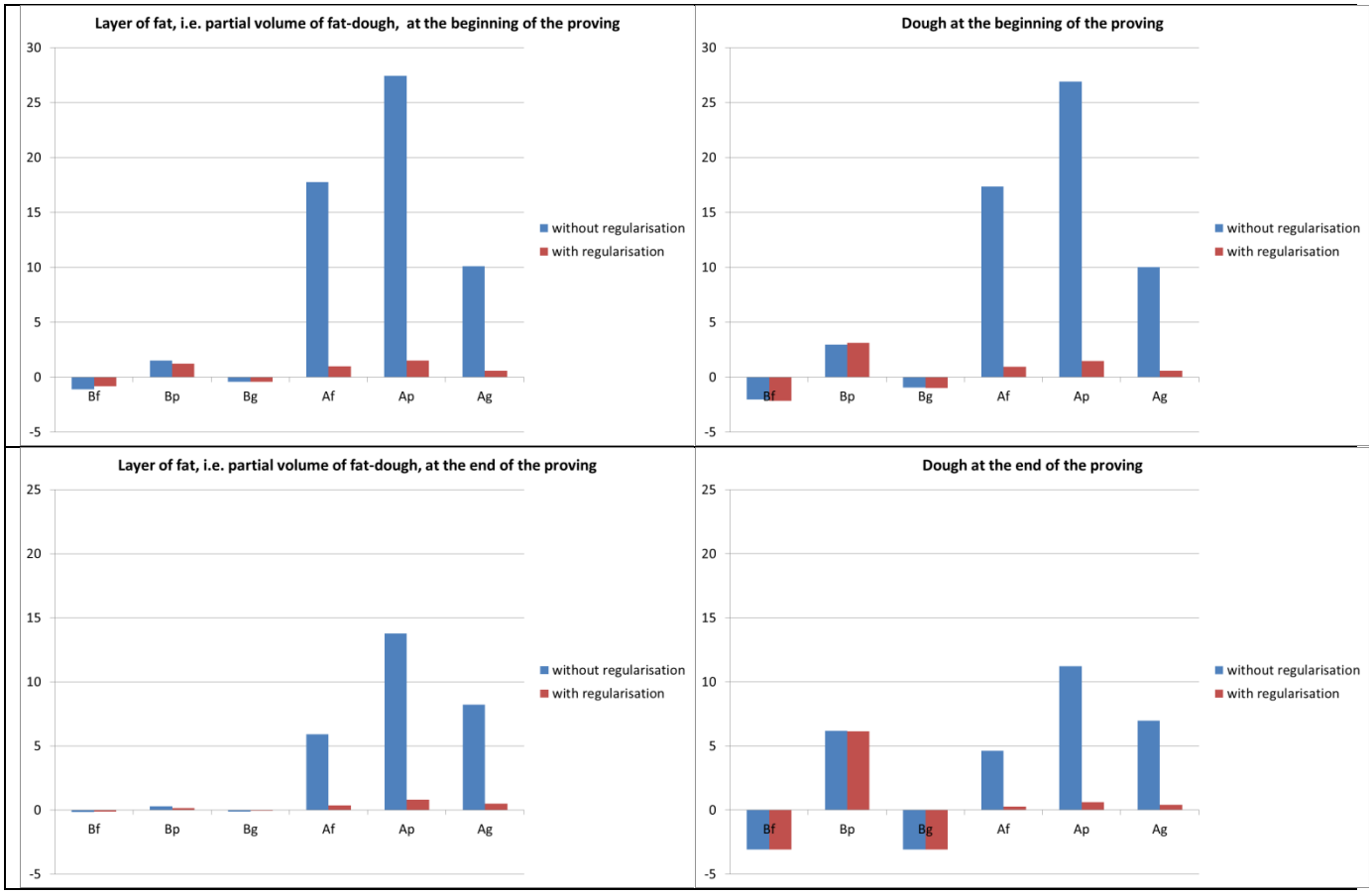

Figure 6: Errors B_i and A_i for a layer of fat (i.e. partial volume of fat-dough) and the dough at the beginning of the proving on the first raw and at the end of the proving on the second raw. The errors are expressed in %. In blue the results without regularisation, in red with regularisation

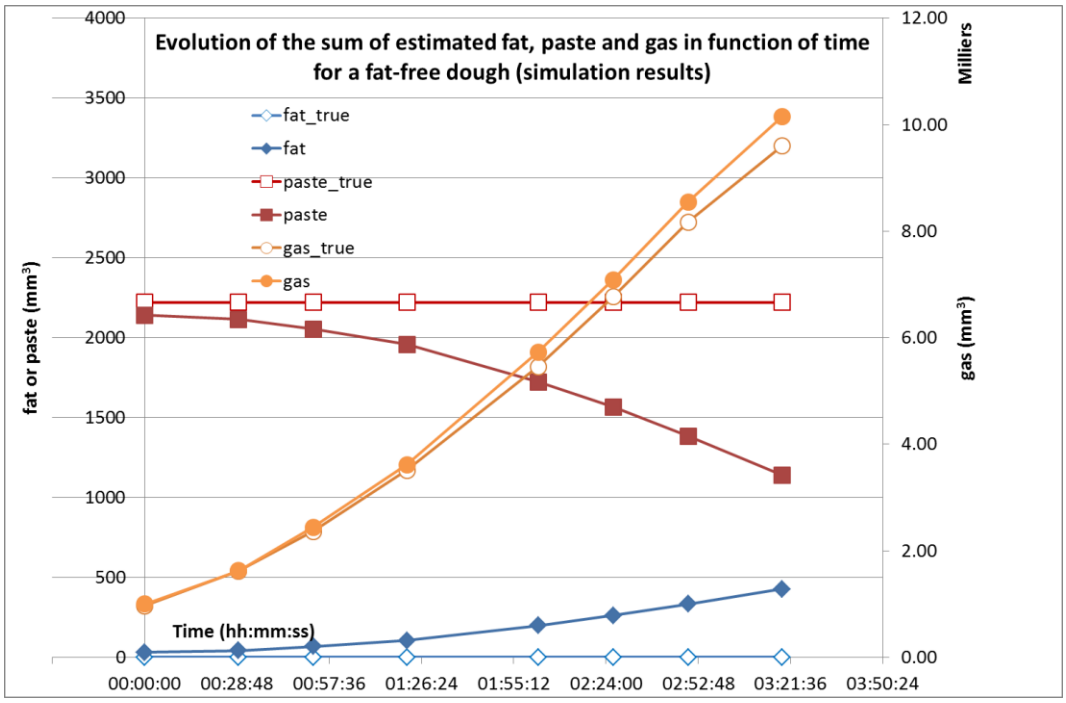

Figure 7: Evolution of the sum of fat, paste and gas in a proving dough in function of time

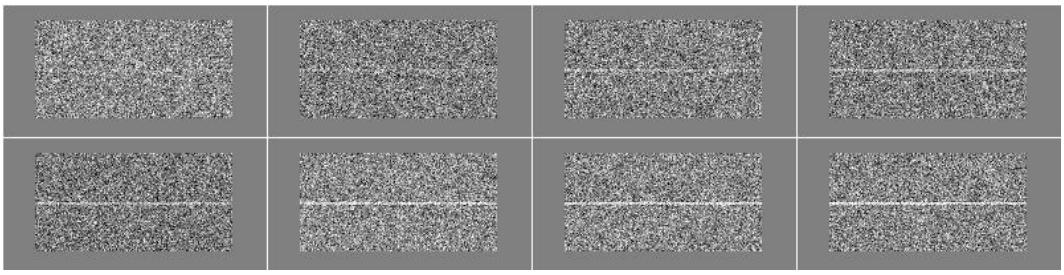

Figure 8: Example of fat maps with different values of contrast. CNR from left to right, top to bottom is 0.4, 0.6, 0.8, 1, 1.2, 1.4, 1.6 and 1.8. The black corresponds to -50%, white to +50%.

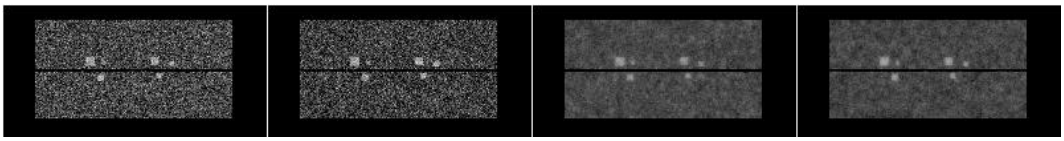

Figure 9: Example of gas maps with different values of contrast. CNR from left to right is 2.5, 3, 4 and 5. The black corresponds to 70%, white to 120%.

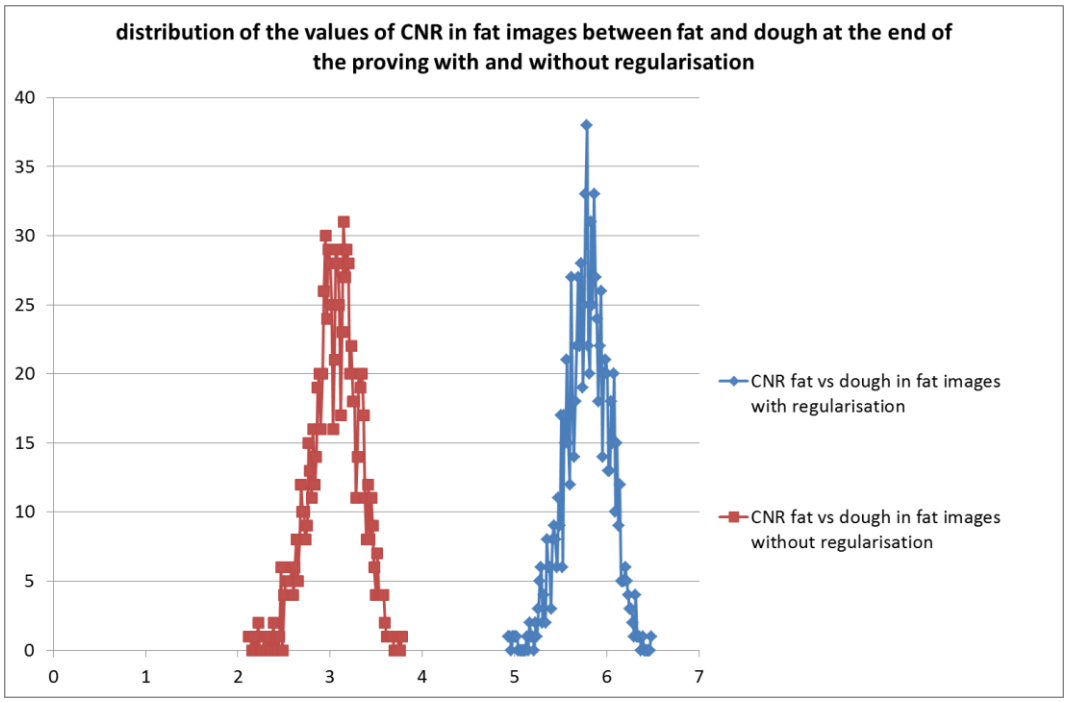

Figure 10: distribution of the values of CNR_f between layers of fat and dough at the end of the proving with and without regularisation. The values were obtained from 1000 Monte-Carlo simulations including the uncertainty on the signal references and on the signal.

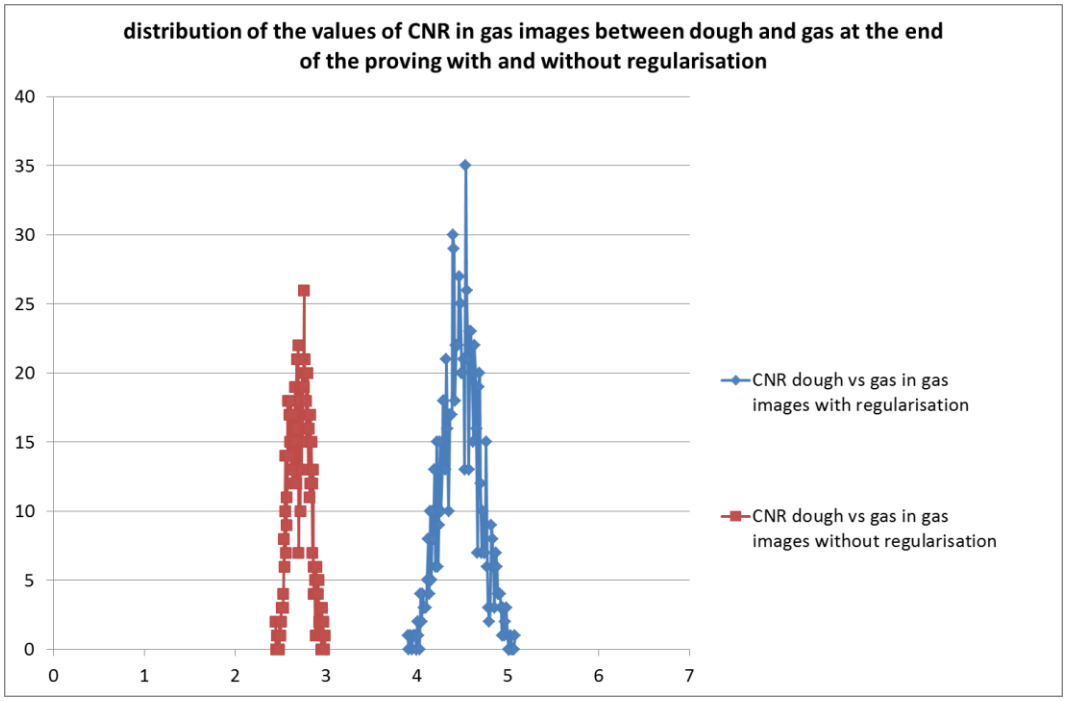

Figure 11: distribution of the values of CNR_g between dough and gas at the end of the proving with and without regularisation. The values were obtained from 1000 Monte-Carlo simulations including the uncertainty on the signal references and on the signal.

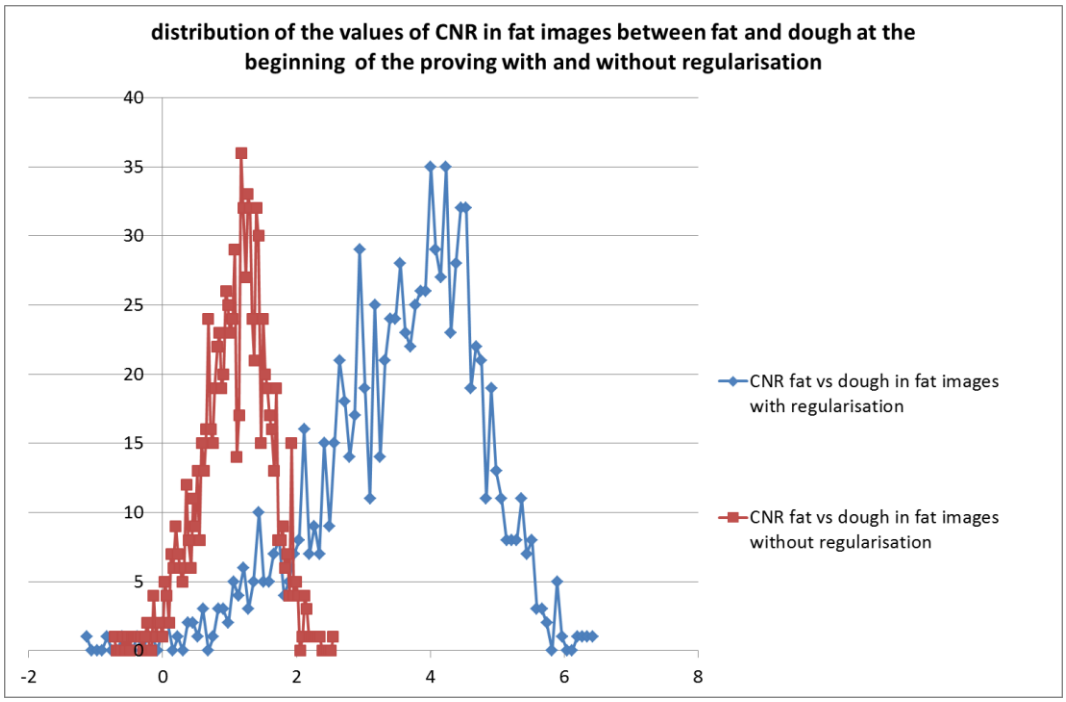

Figure 12: distribution of the values of CNR_f between layers of fat and dough at the beginning of the proving with and without regularisation. The values were obtained from 1000 Monte-Carlo simulations including the uncertainty on the signal references and on the signal

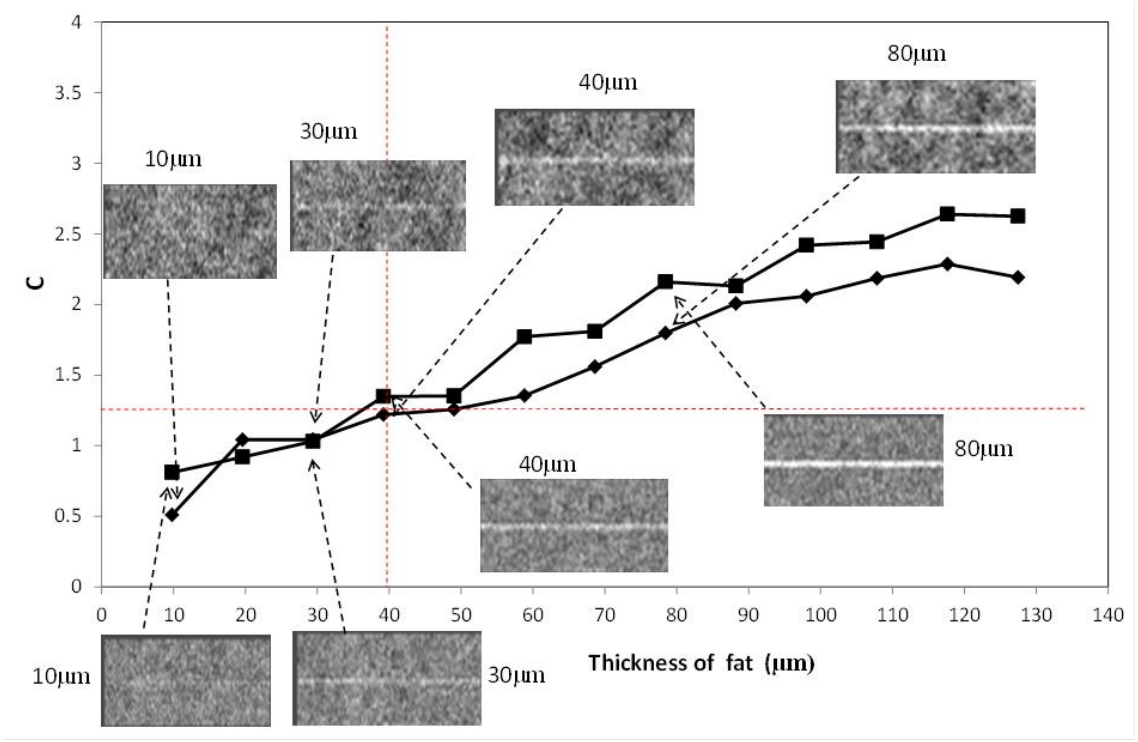

Figure 13: CNR_f between layers of fat and dough at the beginning of the proving for different values of the thickness of the fat layer at the beginning (diamond symbols) and at the end of proving (square symbols); maps of fat proportions at the beginning (top) and at the end (bottom) of proving were superimposed for selected thicknesses of fat layers. The contrast of 1.25 under which the layer is not easily distinguishable corresponds to thickness around 40 µm.